Research Paper

# Gas Separation Properties of Mixed Matrix Membranes Based on Polyimide and Graphite Oxide

Xiao Yuan Chen [1,*], Nguyen Tien-Binh [1], Amaya Romero [2], Antonio Patón [2], Luz Sanchez-Silva [2], Jose Luis Valverde [2], Serge Kaliaguine [1], Denis Rodrigue [1]

[1] Department of Chemical Engineering, Université Laval, Quebec City, QC, G1V 0A6, Canada
[2] Department of Chemical Engineering, University of Castilla La Mancha, Av. Camilo Jose Cela 12, 13071, Ciudad Real, Spain

## Article info

## Keywords

## Highlights

- New type of graphene oxide, thermally reduced graphite oxide (T-RGrO) and ascorbic acid multi-phase reduced graphene oxide (AMP-RGO) were chemically synthesized.
- Control the interlayer distance of graphene nanosheet to improve the gas permeation property of mixed matrix membranes (MMM).
- Graphene/Matrimid MMM have much higher $CO_2/CH_4$ and $H_2/CH_4$ selectivity, could be used for biogas upgrading, naturel gas purification and recovery hydrogen in ammonia plants.

## Graphical abstract



## Abstract

In this work, three different graphene-based materials, namely graphite oxide (GrO), thermally reduced graphite oxide (T-RGrO) and ascorbic acid multi-phase reduced graphene oxide (AMP-RGO), were synthesized and used to produce mixed matrix membranes (MMM) based on Matrimid®5218 for gas separation. From the samples produced, a complete set of characterization was performed including XRD, FTIR, TGA and SEM to relate with the gas separation performance using $H_2$, $CO_2$, $O_2$, $N_2$ and $CH_4$. For all the gases studied, the results showed that membrane permeability was inversely proportional to the gas molecular size. This behavior was associated to multi-phase reduced graphite oxide (AMP-RGO) being an excellent gas barrier for large gas molecules, especially for $CH_4$. The results showed that the $H_2/CH_4$ ideal selectivity increased to 231 which represents a 328% improvement for M/AMP-RGO 0.1 compared to the neat matrix. The $CO_2/CH_4$ selectivity was 79.8 for M/AMP-RGO 0.2 wt.% which represents a 344% improvement compared to the neat polymer. These results confirmed that these membranes can be used for methane separation such as in ammonia plants ($H_2/CH_4$) or biogas upgrading/natural gas purification ($CO_2/CH_4$).

## 1. Introduction

Graphene based materials have attracted a great deal of attention in recent years because of their remarkable electronic, thermal and mechanical properties owing to their unique one-atom-thick structure [1]. For example, the thermal conductivity can be up to 5300 W/m·K which is higher than diamond, with a Young's modulus of 1.0 TPa for a graphene monolayer which is higher than steel and copper [2]. Graphene is currently the thinnest but also the hardest nanomaterial known [3]. Its structure is also very dense as even helium atoms (the smallest gas molecules with a diameter of 2.60 Å) cannot go through graphene, as the carbon-carbon interatomic distances are only 1.42

Å [4]. Therefore, graphene-based materials, such as graphene oxide (GO) and reduced graphene oxide (RGO), have been considered as promising materials for membrane separation minimizing transport resistance and maximizing flux if their stacking structure is carefully controlled [5]. To date, several pioneering works on graphene-based membranes have shown excellent gas separation properties. For example, Kim et al. [6] reported that selective gas ($CO_2$ or $H_2$) diffusion through few-layered GO membranes can be achieved by controlling the gas flow pathways and pores. Synthesis of large-area few-layer graphene by the chemical vapor deposition (CVD)
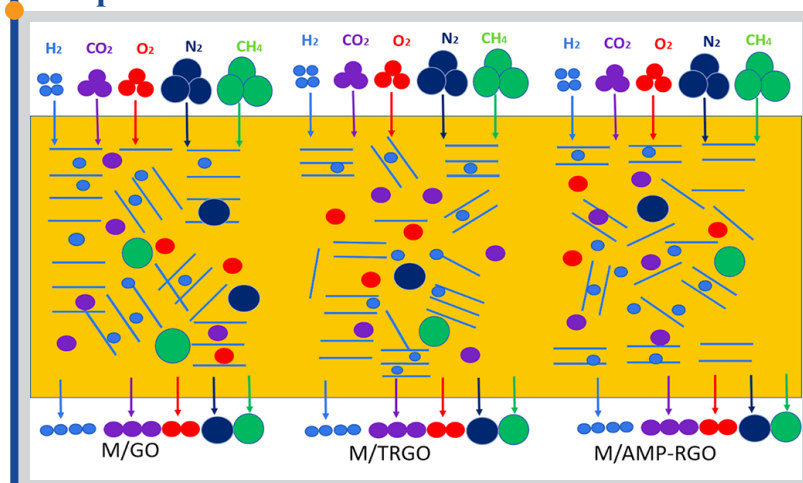
method, and preparation based on polymer-supported materials (poly(1-methylsilyl-1-propyne) (PTMSP)) have shown $H_2$ permeance of 32 GPU and $H_2/CO_2$ selectivity as high as 30. Li et al. [5] developed ultrathin graphene oxide (GO) membranes with thicknesses close to 1.8, 9 and 18 nm on anodic aluminum oxide (AAO) support. These membranes showed gas mixture separation selectivities as high as 2000 for $H_2/CO_2$ at 20 °C. However, the preparation of few-layer graphene membranes is very difficult and time consuming. Furthermore, there are still several challenges for these neat graphene membranes as free-standing GO membranes without substrate/support cannot be used to build separation modules because of their brittleness [7].

On the other hand, polymer-based membrane technology is expected to play a major role in the field of gas separation due to several advantages such as high energy efficiency, low power consumption, easy operation control, easy maintenance and low capital cost [8]. The majority of gas separation modules are made from hollow polymer fibers with different configurations for industrial applications. In the past, cellulose acetate (CA), polysulfone (PSf), polyamide (PA), silicon rubber (SR), polyphenylene oxide (PPO) and polyimide (PI) were often used alone as membrane materials [9]. Today, they are used as matrices and modified using different particles. This led to the development of mixed matrix membranes (MMM) in which inorganic or organic particles, such as carbon-based particles (nanofibers, nanotubes, etc.), ceramics, zeolites and metal organic frameworks (MOF) are introduced in the polymer matrix to improve the gas separation properties [10]. In particular, graphene nanosheets were introduced into gas separation membranes. For example, polyether block amide (PEBA), which is a commercial block copolymer, was filled with GO at different concentrations (0.05, 0.075 and 0.1 wt.%) [11]. The results showed that $CO_2$ permeability increased compared to neat PEBA (from 50 to 100 Barrer) with increasing GO content, while $N_2$ permeability showed negligible variation leading to significant $CO_2/N_2$ selectivity improvement (from 50 to 91) with high operational stability (> 6000 min) at 0.3 MPa and 25 °C. The authors associated their results to the $CO_2$ selective transport channels of GO laminates related to hydrogen bonding between GO and PEBA. These GO nanosheets created several-layered GO stacks leading to a molecular-sieving interlayer spacing and straight diffusion pathways. The same group also studied MMM based on GO (0.1 wt.%) and PEBA with different GO lateral sizes (100-200 nm, 1-2 μm, and 5-10 μm) with thicknesses of approximately 1 nm [12]. The results showed that the 1-2 μm lateral size produced the best $CO_2/N_2$ separation performance with a $CO_2$ permeability of 110 Barrer and a $CO_2/N_2$ selectivity of 80. Dong et al. [13] developed MMM based on partially reduced porous graphene oxide (PRG) nanosheets obtained from graphene oxide (GO) via a wet chemical process for introduction into Pebax®1657. The results showed that these MMM had substantially improved $CO_2$ permeability (from 58 to 119 Barrer) as well as $CO_2/N_2$ selectivity (from 55 to 104) at 0.2 MPa and 30 °C. The $CO_2$ permeability initially increased with increasing the PRG concentration, with the highest $CO_2$ permeability (119 Barrer vs. 58 Barrer for neat Pebax) and $CO_2/N_2$ selectivity of (104 vs. 55 for neat Pebax) at 5 wt.%. The authors assumed that the molecular sieving laminated structures (average width of 0.34 nm) between the neighbouring nanosheets was responsible to create this effective molecular sieving for $CO_2$ against larger gas molecules ($N_2$). Dai et al. [14] used imidazole functionalized graphene oxide (Im-GO) in Pebax®1657 to make MMM for $CO_2$ capture. The membrane filled with 0.8 wt.% Im-GO had the best gas separation performance with a $CO_2/N_2$ selectivity up to 105.5 combined with a $CO_2$ permeability of 76.2 Barrer (25 °C and 0.8 MPa). As mentioned above, several groups used Pebax with GO to produce MMM, but mainly focussed on $CO_2$ capture alone. Furthermore, the results are mostly reported for very low gas pressure as compared in Table 1.

Other groups used GO-based in situ polymerization of polyimide for membrane synthesis [15,16]. For example, Wu et al. [15] synthesized 6FDA-ODA (6FDA: 2,2'-bis-(3,4-dicarboxyphenyl) hexafluoropropane dianhydride, ODA: 4,4'-oxydianiline) using GO or GO modified by polyethylene glycol (PEG) in situ polymerization for $CO_2/N_2$ separation. The best results showed that the $CO_2$ permeability increased from 45 to 250 Barrer, while the $CO_2/N_2$ selectivity increased from 8 to 32 at 1 wt.% of GO modified by PEG 2000. GO and $NH_2$-GO (modified by N,N-dimethylformamide) were introduced in the solvent before the polyimide (BTDA-DMMDA) synthesis reaction [16], (BTDA: 3,3',4,4'- benzophenonetetra-carboxylic dianhydride and DMMDA: 3,3'-dimethyl-4,4'-diamino-diphenyl methane). Then, a series of poly(amic acid) PAA/GO and PAA/$NH_2$-GO suspensions (0-4 wt.%) were used to make MMM. The best permeability for pure $CO_2$ was 8.2 Barrer with a $CO_2/N_2$ ideal selectivity of 35 for PI/GO MMM at 15 °C and 0.1 MPa. For the PI/$NH_2$-GO MMM, a $CO_2$ permeability of 12 Barrer and a selectivity of 38 were obtained for both GO and $NH_2$-GO at 3 wt.%.

Koolivand et al. [17] used Ultem® 1000 polyetherimide (PEI) with graphene-based particles to make MMM of GO/PEI, GO-PEG/PEI and GO-$NH_2$/PEI nanosheets (0.25, 0.5 and 0.75 wt.%). GO-PEG and GO-$NH_2$

nanosheets were modified by reacting pristine GO with polyethylene glycol and ethylene diamine, respectively. Compared to neat PEI ($P_{CO2}$ of 2.4 Barrer and $CO_2/CH_4$ selectivity of 25.8), all the MMM permeabilities (for both $CO_2$ and $CH_4$) decreased while selectivities increased. The results showed that GO-$NH_2$ containing membranes were more effective at separating gases based on both size and solubility differences. For example, the 0.75 wt.% GO-$NH_2$/PEI had 1.57 Barrer of $CO_2$ permeability and $CO_2/CH_4$ selectivities up to 142 at 25 °C and 10 bar. The same group compared the effect of graphene oxide (GO) nanosheets on the $CO_2/CH_4$ separation performance of a rubbery polydimethylsiloxane (PDMS) membrane, as well as glassy polyetherimide (PEI) [18]. The best results were obtained at 0.25 wt.% GO for which simultaneous improvement in $CO_2$ permeability (2.7 Barrer, 16% increase) and $CO_2/CH_4$ selectivity (41, 59% increase) was obtained. Also, simultaneous improvement of $CO_2$ permeability (5076 Barrer, 29%) and $CO_2/CH_4$ selectivity (8.7, 112%) was observed for the PDMS membrane using 0.5 wt.% GO at 10 bar and 25 °C.

Feijani et al. [19] prepared MMM adding graphene oxide (GO) in polyvinylidene fluoride (PVDF) or chemically modified PVDF (M-PVDF). For PVDF/GO compared to the neat PVDF membrane, the permeability of He, $CO_2$, $N_2$ and $CH_4$ decreased by 14%, 4%, 56% and 45% respectively, by incorporating 1 wt.% of GO, while the He/$CH_4$, He/$N_2$ and $CO_2/CH_4$ selectivities increased by 94%, 34% and 118%, respectively. For the M-PVDF/GO membranes, the permeability of all gases increased with the addition of 0.25 and 0.5 wt.% of GO. The $CO_2/CH_4$ selectivity increased by 10% and 22% at 0.25 and 0.5 wt.% of GO respectively, compared to the neat M-PVDF.

Ha et al. [20] introduced GO (8 wt.%) into PDMS leading to a 99.9% permeability reduction for $H_2$, $O_2$, $N_2$, $CH_4$ and $CO_2$ at 35 °C and 10 atm. A significant increase of the ideal selectivities was observed for $CO_2/N_2$ and $CO_2/CH_4$ for which 2.5 and 3.2 times improvement were observed compared to neat PDMS. Also, $H_2$ permeability was decreased from 1000 to 10 Barrer, but $H_2/N_2$ and $H_2/CH_4$ selectivities were still very low (10 and 2).

Introduction of amino acid-functionalized graphene oxide (GO-DA-Cys) nanosheets into a sulfonated polyether ether ketone (SPEEK) MMM was done by Xin et al. [21]. The optimum separation performance was achieved at a GO-DA-Cys content of 8 wt.% with selectivities of 49 and 60 for $CO_2/CH_4$ and $CO_2/N_2$ respectively, while a $CO_2$ permeability of 22 Barrer at 1.5 bar and 25 °C was obtained.

Carbon nanotubes (CNT) and graphene oxide (GO) in Matrimid were shown to improve the $CO_2$ separation performance of the neat membranes. For example, Li et al. [22] reported that a combination of CNT and GO produced a synergistic effect on the membrane permselectivity. The highly smooth CNT walls acted as a gas highway producing high permeability, while the graphene oxide nanosheets acted as a selective barrier producing high selectivity through the hydroxyl and carboxyl groups on the GO surface. The best results were obtained by combining 5 wt.% of CNT with 5 wt.% of GO (Matrimid-CNT/GO-5/5) with a $CO_2$ permeability of 38 Barrer, a $CO_2/CH_4$ selectivity of 84.6 and a $CO_2/N_2$ selectivity of 81. This is to be compared with 10 wt.% GO which gave a $CO_2$ permeability of 6.5 Barrer, a $CO_2/CH_4$ selectivity of 70 and a $CO_2/N_2$ selectivity of 65. All the measurements were performed at 30 °C and 2 bar. Unfortunately, no information on other gases was provided.

Melicchio et al. [23] prepared graphene oxide (GO) 2.2 wt.% dispersed in Matrimid® 5218 and compared the gas permeability between neat PI and two isotropic membranes by different preparation methods: thin film membrane (TFM) and thick isotropic film (TIF). The results showed that TFM have very low permeability (4.5, 5.4, 1.9, 2.0 and 2.4 Barrer for He, $H_2$, $CO_2$, $O_2$ and $N_2$), while TIF have much higher permeability (330, 322, 160, 131 and 197 Barrer for He, $H_2$, $CO_2$, $O_2$ and $N_2$) compared to neat Matrimid. However, all these membranes have almost no selectivity (less than 2).

From the above information, almost all the work in the present literature focussed on $CO_2/CH_4$ and $CO_2/N_2$ separation and the MMM were based on commercial polymers like Ultem 1000 (PEI), PVDF, Matrimid and PDMS. But PDMS is a rubbery polymer and its permeability strongly depends on the relative solubility of each gas molecule; i.e. the solubility selectivity is often higher than the diffusivity selectivity. Therefore, PDMS is more permeable to large, soluble and condensable gases ($CO_2$) than smaller and less condensable gases ($H_2$). Therefore, PDMS is not a good choice for hydrogen recovery. On the other hand, Ultem and PVDF have very low permeability for all gases. But Matrimid® 5218 has good thermal stability, mechanical properties and gas transport properties, especially for hydrogen recovery and $CO_2/CH_4$ separation.

Based on the results reported on graphene oxide addition in polymer membranes, different treatments were used to control the distance between the particle layers and to determine the concentration effect on the MMM barrier properties using different gas molecules ($H_2$, $CO_2$, $O_2$, $N_2$ and $CH_4$).

**Table 1**
Gas permeability data for polymer/GO MMM from literature.

| Membrane (polymer/GO) | GO content (wt.%) | $P_{CO_2}$ (Barrer) | $\alpha_{CO2/CH4}$ (-) | $\alpha_{CO2/N2}$ (-) | Test conditions (ºC / bar) | Ref. |
|---|---|---|---|---|---|---|
| PEBA/GO | 0.1 | 50-100[a] | | 50-91 | 25 / 3 | [11] |
| PEBA/GO | 0.1 | 50-110 | | 50-80 | 25 / 3 | [12] |
| Pebax®1657/PRGO | 5.0 | 58-119 | | 55-104 | 30 / 1-5 | [13] |
| Pebax®1657/GO | 0.8 | 76.2 | | 105 | 25 / 9 | [14] |
| 6FDA-ODA/PEG-GO | 1.0 | 45-250 | | 8-32 | 30 / 10 | [15] |
| BTDA-DMMDA/NH$_2$-GO | 3 | 8.2-12 | | 35-38 | 15 / 1 | [16] |
| PEI/NH$_2$-GO | 0.75 | 2.4-1.57 | 25.8-142 | | 25 / 10 | [17] |
| PDMS/GO | 0.25 | 5076 | 8.7 | | 25 / 10 | [18] |
| PVDF/GO | 0.5 | 0.897 | 40.6 | | RT / 5 | [19] |
| M-PVDF/GO | 0.5 | 1.5 | 31.5 | | RT / 5 | [19] |
| PDMS/GO | 8 | 3800-27.7 | | 9.5-24 | 35 / 10 | [20] |
| SPEEK/GO | 8 | 22 | 49 | 60 | 25 / 1.5 | [21] |
| Matrimid/GO | 10 | 8.8-6.5 | 34-70 | 33-65 | 30 / 2 | [22] |
| Matrimid/GO | 2.2 | 45.7-160 | | 0.52-0.81 | RT / 0.1 | [23] |

a: for example 50-100, 50 for neat polymer, 100 for MMM. RT: room temperature

## 2. Experimental

### 2.1. Materials

Matrimid® 5218 in a powder form was obtained from Huntsman Advanced Materials Americas Inc (USA). Chloroform as solvent and graphite powder (<20 μm) were supplied by Sigma-Aldrich (Spain). Potassium permanganate (KMnO$_4$), sulfuric acid (H$_2$SO$_4$), hydrogen peroxide (H$_2$O$_2$) and ethanol (CH$_3$CH$_2$OH) with a purity of 99%, 96%, 99.5% and 99.5% respectively, and 37% AR grade of hydrochloric acid (HCl) were supplied by PANREAC (Spain). Ascorbic acid with a purity of 99% was supplied by VWR (Spain).

### 2.2. Methods

#### 2.2.1. Graphite oxide synthesis (GrO)

Graphite oxide was synthesized following the improved Hummers method with slight modifications [24]. A mixture of 15 g of graphite and 45 g of KMnO$_4$ (oxidizer) was slowly added to 400 mL of H$_2$SO$_4$ under constant agitation. The mixture was maintained at 50 ºC for 3 h. Then, the mixture was added to a beaker containing 400 g of flake ice and 3 mL of H$_2$O$_2$ to stop the oxidation reaction. The mixture was filtered under vacuum and washed with 200 mL of deionized water, HCl and CH$_3$CH$_2$OH. Finally, the compact cake was dried overnight at 100 ºC. The obtained product was designated as graphite oxide (GrO). Graphene oxide (GO) synthesis was carried out by

sonication (50% amplitude and a complete cycle) at room temperature of a mixture of 800 mg of graphite oxide and 800 mL of deionized water. The final mixture was centrifuged and the obtained solid was dried overnight at 80 °C. Figure 1 presents a schematic of this process.

#### 2.2.2. Thermally reduced graphite oxide (T-RGrO) synthesis

Thermal reduction was carried out by introducing 5 g of graphite oxide in a laboratory oven at low temperature (T<300 ºC). The carbon material expansion took place after a certain time (20-40 min) separating the graphene layers and removing some oxygen functional groups from the structure. The obtained product was designated as thermally reduced graphite oxide (T-RGrO).

#### 2.2.3. Ascorbic acid multiphase reduced graphene oxide (AMP-RGO) synthesis

Chemical reduction of graphite oxide was carried out using ascorbic acid due to its innocuous and environmentally friendly character. Ascorbic acid multiphase reduced graphene oxide (AMP-RGO) synthesis was carried out by mixing 800 mg of T-RGrO in 800 mL of deionized water with 800 mg of ascorbic acid. The chemical reduction was performed under constant agitation for 48 h at room temperature [24,25]. After reduction, the solution was centrifuged and the obtained product was filtered and washed several times with deionized water (until pH=7) to remove the remaining acid. Finally, the solid obtained was dried overnight at 80 ºC.
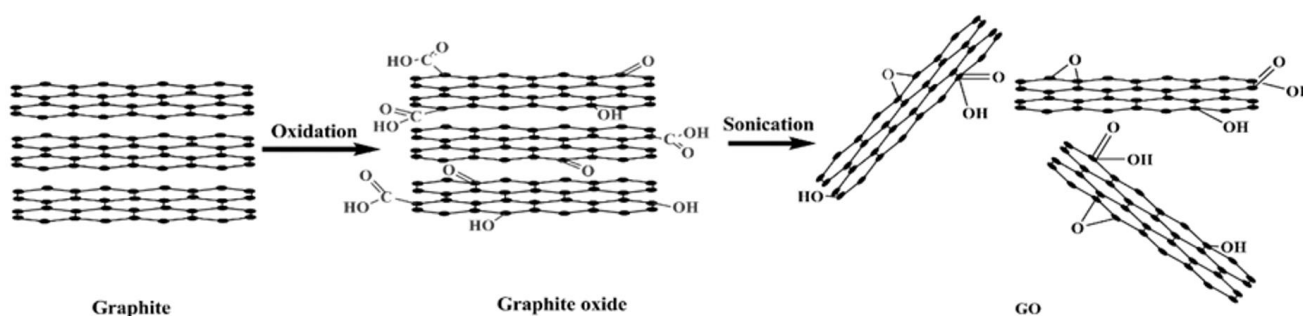


**Fig. 1.** The chemical route from graphite to graphene oxide.

### 2.3 Mixed matrix membrane preparation

A mixture of a specific amount of graphite oxide was prepared in 20 mL of chloroform and introduced in a liquid cooled jacketed reactor to maintain the solution at room temperature. The mixture was sonicated (UP400S, Hielscher, 400 W/24 kHz, 50% amplitude and a complete cycle) for 1 h to separate the graphene sheets of graphite oxide and obtain graphene oxide (GO) [26]. Then, approximately 10% of the Matrimid powder was added to the GO suspension. The slurry was agitated for 1 h and, after good homogenization, the remaining amount of the polyimide powder was added and the final slurry was agitated again for 1-2 h. Solvent was evaporated to obtain a 10-12 wt.% solution. For degassing, the polyimide solutions were left in a hood for 30 min. A nascent film was cast with the solution onto a clean glass plate using a small metal container with a cover to delay solvent evaporation from the nascent membrane. After 24 h, the cover was removed to evaporate residual solvent for another 24 h. Then, the films were placed in a vacuum oven at 100 °C and each membrane was annealed for 4 h. Finally, the films were slowly cooled down to room temperature (RT) and stored in a desiccator before characterization. Each MMM was coded as M/GOx where x is the graphite oxide weight percent. Matrimid composites with TRGO and AMP-RGO membranes were coded as M/T-RGO and M/AMP-RGO and were produced using the same method.

### 2.4. Characterization

Elemental analysis was performed using energy-dispersive X-ray spectroscopy (EDX) analysis on a scanning electron microscope (SEM) JEOL JSM-840A. Powder X-ray diffraction (XRD) analysis was performed on a diffractometer (PHILIPS, PW-1711) with a Cu Ka radiation (k = 1.5404 Å). The samples were scanned at a rate of 0.02º/step over the range $5º \leq 2\theta \leq 90º$ (scan time = 2 s/step) and the diffractograms were compared with PDF-ICDD references. Different parameters can be obtained from XRD. The interlaminar space ($d_{002}$) was obtained using Bragg's equation:

$$d_{002} = \frac{\lambda}{2 \sin \theta} \tag{1}$$

where $\lambda$ is the radiation wavelength ($\lambda = 0.15404$ nm) and $\theta$ is the diffraction peak angle (º).

The packing size ($L_c$) of graphene planes was calculated by the Debye-Scherrer equation as [27,28]:

$$L_c = \frac{K \lambda}{FWHM \cos\theta} \tag{2}$$

where $FWHM$ is the width at half height of the diffraction peak and $K$ is the form factor ($K = 0.9$).

The number of graphene layers ($N_c$) in a crystal is directly proportional to their packing degree and inversely proportional to the distance between them ($d_{002}$) to give:

$$N_c = \frac{L_c}{d_{002}} \tag{3}$$

The FTIR spectra were recorded using a Nicolet Magna 850 Fourier transform infrared spectrometer (Thermo Scientific, USA) equipped with a liquid-nitrogen cooled narrow-band MCT detector using Golden-Gate (diamond IRE) ATR accessories (Specac Ltd., U.K.). Each spectrum was obtained from the acquisition of 128 scans at 4 cm⁻¹ resolution from 4000 to 700 cm⁻¹ using Happ-Genzel apodization. All spectral operations were executed using the GRAMS/AI 8.0 software (Thermo Galactic, USA).

The weight curves (TGA-DTG) were recorded using a model Q5000IR (TA Instruments, USA) from 50 to 1000 °C at a heating rate of 10 °C/min under a nitrogen atmosphere.

The glass transition temperature and Young's modulus were determined using a dynamic mechanical thermal analyzer RSA-3 (TA Instruments, USA) at a frequency of 1 Hz. The temperature was increased from 50 to 350 °C at a rate of 10 °C/min with a strain of 0.05%. Membrane thickness was measured by a micrometer (Starrett No. 732, USA). All the membranes had a thicknesse between 50 and 80 mm and the other dimensions were 25 x 6 mm². 

Scanning electron micrographs (SEM) were recorded to determine the crystallite size and to characterize the materials dispersion state. Images were taken on a JSM-840A (JEOL, Japan) operated at 15-20 kV.

### 2.5. Gas permeation measurements

The pure gas transport properties were measured by the variable pressure (constant volume) method [9,29]. The permeability coefficient, P (cm³ (STP) cm/cm² s cmHg) and the ideal selectivity were obtained. In the measurement, the permeate pressure was allowed to vary from $10^{-3}$ to 30 Torr. For each composition, at least three different membranes were prepared to detect defective membranes which would yield inacceptable permeation rates. All of the reported data were established for at least two replicas of the same membrane. More details on the experimental set-up and calculations can be found in our previous work [9,29,30].

## 3. Results and discussion

### 3.1. Characterization of the different graphene-based materials and the mixed matrix membranes

#### 3.1.1. Elemental analysis and XRD characterization

Table 2 presents the oxygen and carbon content (wt.%) of the different graphene-based materials. Graphite, the non-oxidized raw material, is composed of 100% carbon atoms as expected. After the oxidation process to obtain graphite oxide (GrO), the oxygen content as part of a functional group increased to 52%. But after the thermal reduction process, the oxygen content decreased to 37% (T-RGrO). AMP-RGO, obtained from a combined thermal and ascorbic acid chemical reduction, only has 27% of oxygen groups [26].

**Table 2**
Elemental analysis of graphite, graphite oxide (GrO), thermally reduced graphite oxide (T-RGrO) and ascorbic acid multiphase reduced graphene oxide (AMP-RGO).

| Material | Graphite | GrO | T-RGrO | AMP-RGO |
|---|---|---|---|---|
| Oxygen content (wt.%) | 0 | 52 | 37 | 27 |
| Carbon content (wt.%) | 100 | 48 | 63 | 73 |

**Table 3**
XRD parameters of graphite and graphene-based materials.

| Materials | 2θ (º) | $L_c$ (nm) | $d_{002}$ (nm) | $N_c$ |
|---|---|---|---|---|
| Graphite (G) | 26.7 | 37.1 | 0.34 | 111 |
| Graphite oxide (GrO) | 9.96 | 5.62 | 0.89 | 6 |
| Thermally reduced graphite oxide (T-RGrO) | 23.7 | 0.92 | 0.39 | 3 |
| Ascorbic acid multiphase reduced graphene oxide (AMP-RGO) | 22.1 | 0.97 | 0.41 | 2 |

The XRD analysis results for the graphene-based materials are presented in Figure 2. The characteristic parameters derived from the diffractograms are reported in Table 3. Graphite showed a [002] peak at a 2θ value of 26.7º which is consistent to a layer separation ($d_{002}$ from Eq.1) of 0.34 nm and a number of layers of around 111. After oxidation, the [002] peak disappeared and a new one appeared at 2θ = 10º. As a consequence, the interlayer distance ($d_{002}$) clearly increased while the crystal stack height ($L_c$ in Eq.2) decreased after oxidation. Larger distance was attributed to the expansion caused by the presence of oxygen functional groups and water molecules located in the interlayer galleries of the hydrophilic GrO samples. Then, $d_{002}$ decreased after reduction for T-RGrO. Finally, the number of layers in the stacking structure ($N_c$) substantially decreased after graphite oxidation. After thermal and multiphase reduction, T-RGrO and AMP-RGO showed similar XRD patterns with the main peak centered at 2θ = 23.7 º and 22.1º respectively, while the interlayer distance and crystal domains ($L_c$) decreased after both reduction types due to higher structural disorder. AMP-RGO was treated by ascorbic acid to reduce T-RGrO and the hydrazine attacks the structure more intensely, so the crystal domains were slightly higher in AMP-RGO than T-RGrO. Finally, the number of layers in the stacking structure ($N_c$) decreased to 3 and 2, as expected [31].
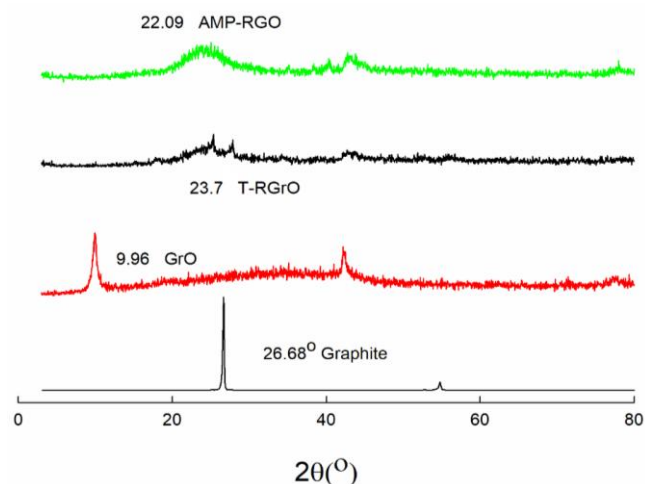
**Fig. 2.** X-ray diffraction (XRD) analysis of graphite, GrO, T-RGrO and AMP-RGO.

The XRD pattern of Matrimid shows broad peaks at $2\theta$ of 14.2, 17.5 and 25.8° in Figure 3. This can be attributed to the amorphous nature of the polymer in agreement with literature [32]. In MMM containing GO, the peak at 17.5° is shifted to 16.7° as GO layers can act as nucleating points increasing the polymer crystallinity. Furthermore, in spite of GO loading in membranes, the characteristic feature of GO at a $2\theta$=9.96° disappeared in the MMM XRD spectra. This shows that since the GO layers were far enough from each other in the polymer matrix, there was no GO peak observed. Therefore, fully exfoliated and dispersed GO layers in Matrimid membranes were achieved as reported by Feijani et al. [19].
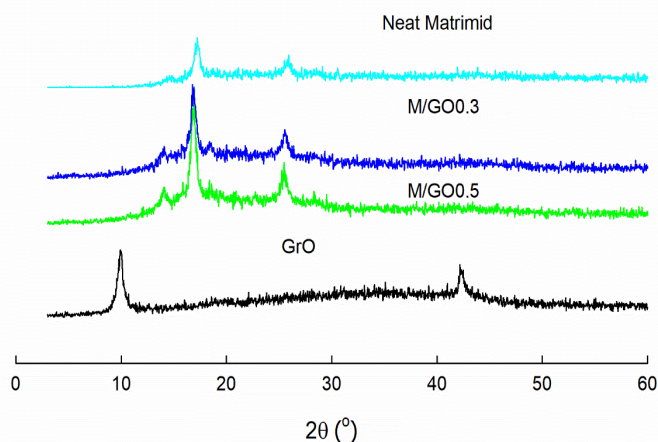


**Fig. 3.** X-ray diffraction (XRD) analysis of GrO, neat Matrimid and mixed matrix membranes (M/GO).

### 3.1.2. FTIR characterization

FTIR analyses of the membranes are presented in Figure 4. The characteristic bands around 1775 cm$^{-1}$ (asymmetric stretching of C=O in the imide group), 1710 cm$^{-1}$ (symmetric stretching of C=O in the imide group), 1365 cm$^{-1}$ (stretching of C-N in the imide group), and C-H group at 720 and 3000 cm$^{-1}$ are representative peaks of Matrimid. The bands around 700-900 cm$^{-1}$ are attributed to (C-H), C-O-C anhydride group appears at 1050 cm$^{-1}$, while the C-O band at 1275 cm$^{-1}$ and C=O band at 1720-1780 cm$^{-1}$ present in GrO, TRGO and AMP-RGO, were hidden by the groups in Matrimid. The C-OH hydroxyl group was not detected in M/GO membranes probably due to the low GO content used. Therefore, all the MMM have very similar peaks (Figure 4).
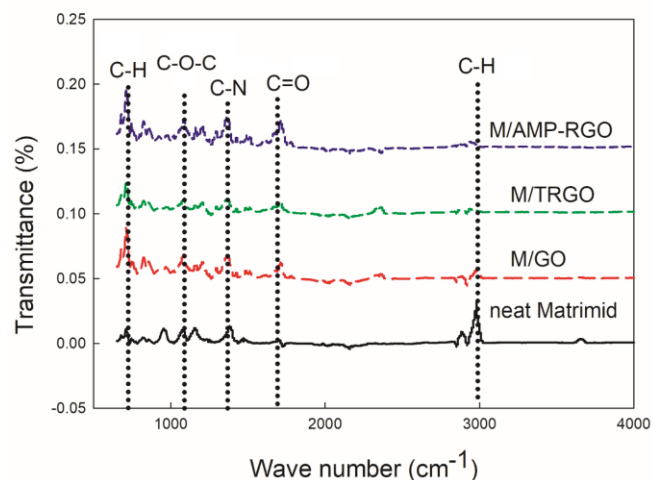


**Fig. 4.** FTIR spectra of the MMM.

### 3.1.3. Thermal characterization

Figure 5 (left) shows the TGA and DTG profiles corresponding to graphite oxide (GrO), thermally reduced graphite oxide (T-RGrO) and ascorbic acid multiphase reduced graphene oxide (AMP-RGO). In the graphite oxide TGA curves, three different weight loss steps can be seen. The first one, between 0 and 200 ºC, is mainly due to the elimination of both water and solvent molecules as well as the decomposition of the more labile oxygen functional groups [33]. The second weight loss step, between 200 and 500 ºC, is related to the removal of the more stable oxygen groups. Finally, the third step (above 500 ºC) is associated to the material thermal degradation.

Multiphase reduced sample (AMP-RGO) did not show significant weight loss during the first step, confirming the elimination after reduction of almost all the labile functional groups and water molecules. The thermally reduced sample (T-RGrO) only lost 5% initially, while 20-23% was lost in the second step indicating that most of the more stable oxygen groups remained in the structure after thermal reduction. Finally, thermal degradation started at around 600 ºC showing a third step weight loss of around 35% [34]. Approximately 45% did not decomposed until 1000 ºC showing its high thermal stability. For AMP-RGO, the curve showed that the degradation was steady with increasing temperature. Finally, more than 60% carbon did not degrade until 1000 ºC under a nitrogen atmosphere.

Figure 5 (right) presents the TGA results for MMM. The temperatures to reach 5% (T$_{d5\%}$) and 10% (T$_{d10\%}$) weight loss in TGA are usually reported to characterize the membrane's thermal stability. In all cases, the T$_{d5\%}$ were above 233 ºC and the T$_{d10\%}$ above 450 ºC. The thermal stability of the Matrimid/GO-based MMM is therefore considered to be sufficient for most gas separation applications [35]. The DTG curves also give information on the pyrolysis rates. In these curves, three steps can be seen: one at low temperature (around 250 ºC) related to residual solvent or hydroxyl groups; the second (520-540 ºC) fast weight decrease is related to the polymer degradation, while H$_2$, CO, CO$_2$ and CH$_4$ evolve from the sample; the third step (570-700 ºC), with a slow weight decrease, is usually associated with residual non-elementary carbon components [36].

### 3.1.4. Morphology characterization

Figure 6 presents the morphology of the different materials studied. Graphite oxide (GrO) and thermally reduced T-RGrO showed well-defined sheets. After the oxidation process, GrO samples present a damaged structure. AMP-RGO showed a single flake structure with relatively large surface similar to a thin curtain which indicates that very good exfoliation took place after the oxidation process and reduction.
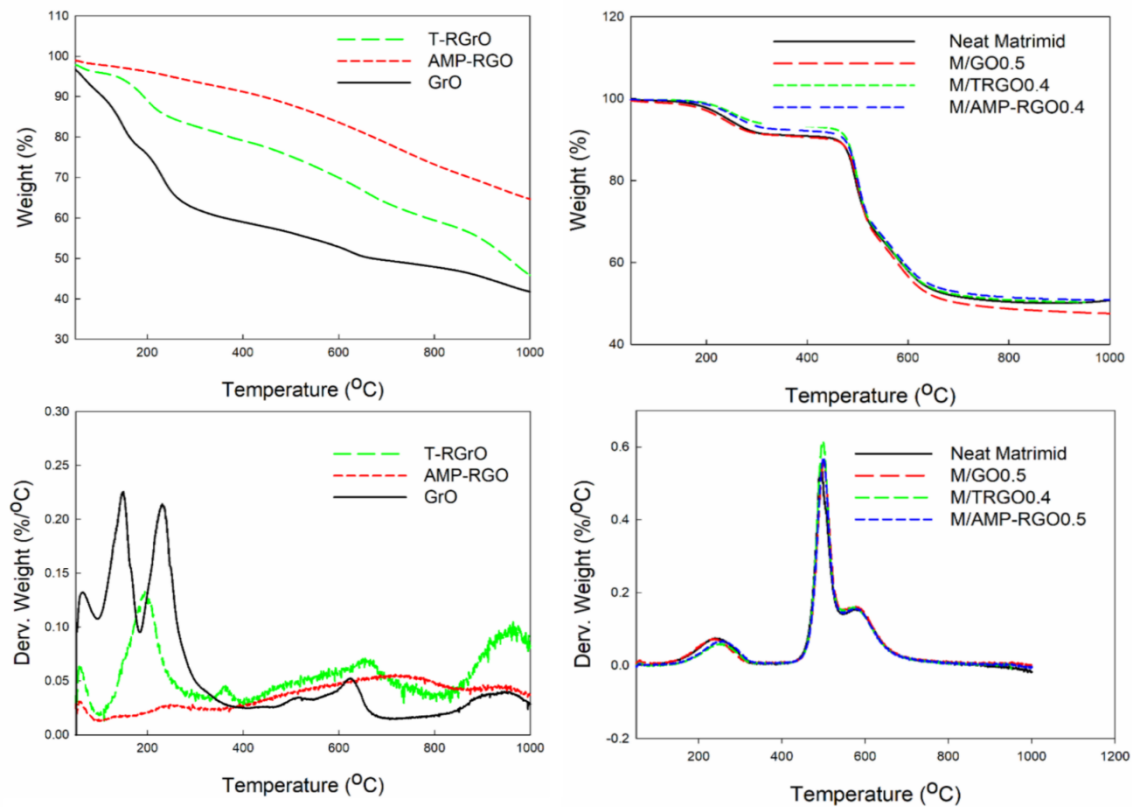
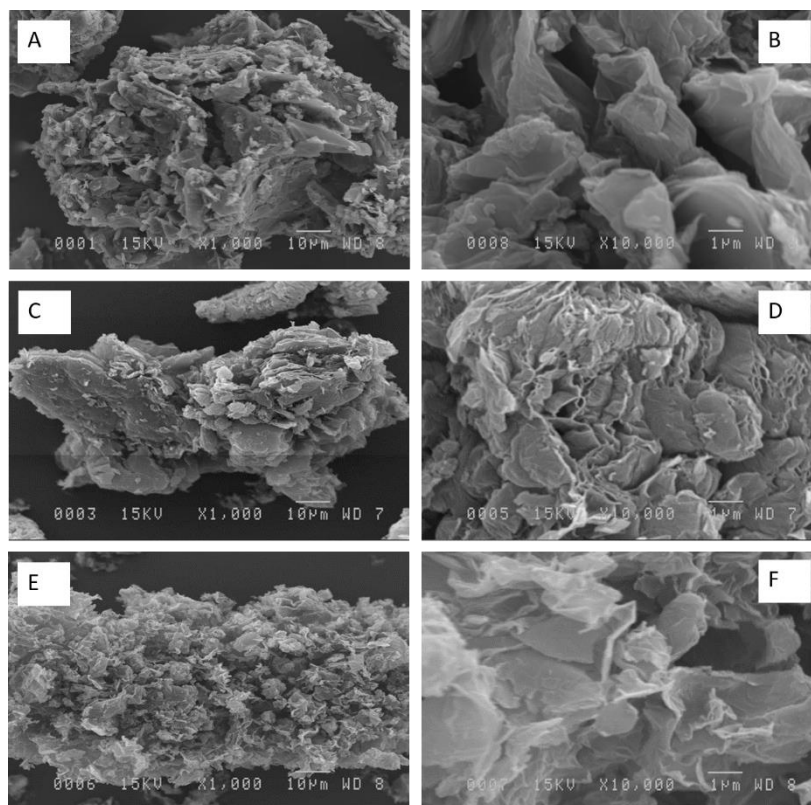**Fig. 5.** TGA and DTG curves of the graphene-based materials (left) and MMM (right).



**Fig. 6.** SEM images of graphite oxide (GrO) (A, B), thermally reduced graphene oxide (T-RGrO) (C, D) and ascorbic acid multiphase reduced graphene oxide (AMP-RGO) (E, F) samples.

Figure 7 presents the cross-section images of graphene composites membranes (A-C) and neat Matrimid membrane (D). Figure 7 also presents MMM at the same graphene content (0.4 wt.%) for the three types: M/GO0.4 (A), M/TRGO0.4 (B) an M/AMP-RGO0.4 (C). These images show that the graphene spatial distribution is quite uniform and the polymer-particle interface is of good quality. Each particle is in the center of a polymer alveolus. Obviously, these alveoli in Figures 7 (A, B and C) are not present in Figure 7 (D). The shape and size of these alveoli are related to the interaction between the polymer and the inorganic particles [8]. Another point of interest is that the number of alveoli in the images at the same magnification is in the following order: A (26) < B (38) < C (48). (From the cross-section images in

Figure 7, it may be seen that each alveolae bears one particle. Therefore, the number of alveoli is equal to that particles.) This indicates that GO (A) dispersion was less than TRGO, and that AMP-RGO had the best dispersion meaning that the number of GO graphene layers is higher than TRGO and AMP-RGO. This is consistent with the XRD analysis (Table 2) where the layer number was found to be 6, 3 and 2 for GrO, TRGO and AMP-RGO, respectively.

Figure 8 compares the cross-section MMM morphology with different T-RGO contents (0.2, 0.3, 0.4 and 1 wt.%). Images A-C show that a uniform graphene distribution was achieved, while image D presents some agglomeration known to form non-selective defects in MMM [37].
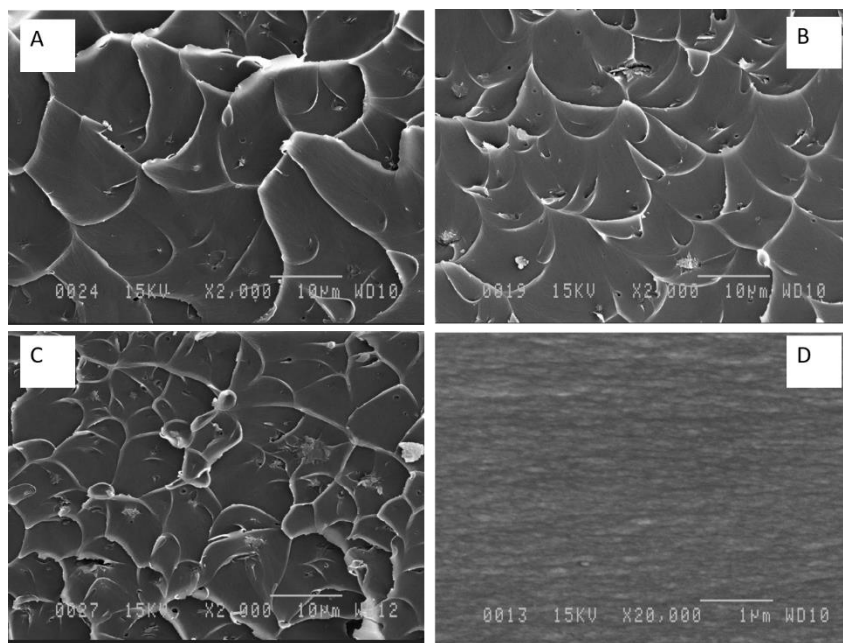


**Fig. 7.** Cross-section SEM images of: (A) M/GO0.4, (B) M/T-RGO0.4, (C) M/AMP-RGO0.4 and (D) neat Matrimid.
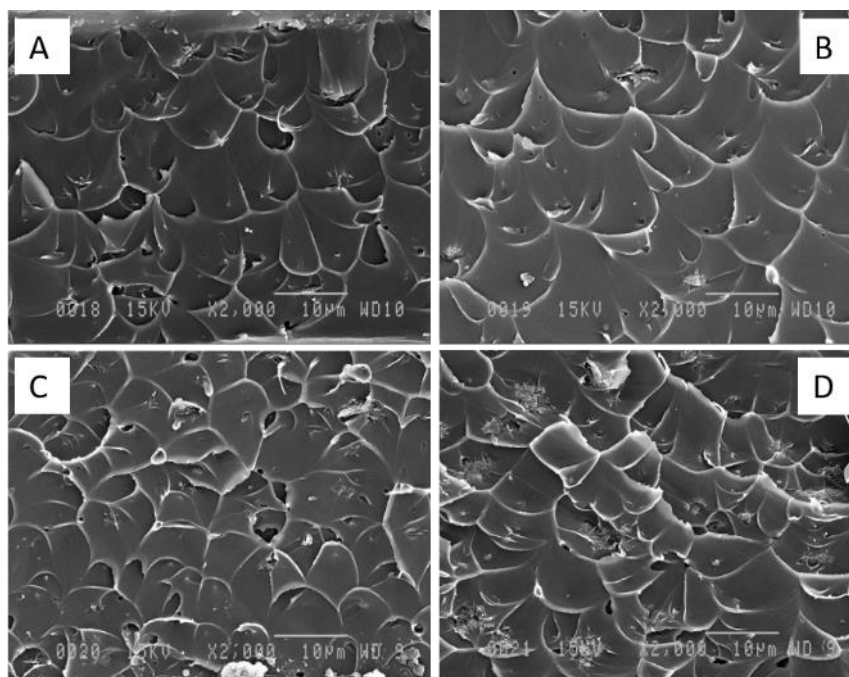


**Fig. 8.** Cross-section SEM images of: (A) M/T-RGO0.2, (B) M/T-RGO0.3, (C) M/T-RGO0.4 and (D) M/T-RGO1.

### 3.1.5. Dynamic mechanical characterization

Given the excellent Young's modulus of graphene (1.0 TPa for a graphene monolayer), it can be expected that the MMM mechanical properties would increase based on the good (homogeneous) dispersion in the membrane produced. For instance, the Young's modulus increased from 2.26 GPa for neat Matrimid to 2.40 GPa for M/GO0.1, but a loss of elongation at break from 49 to 9.8% is also obtained (see Table 4). For M/TRGO and M/AMP-RGO MMM, the Young's modulus and strength also increased and the elongation at break decreased to different level (see Figure 9). Generally, strong interactions between GO-based graphene and the polymer matrix can restrict the polymer chain mobility leading to more rigid, but more brittle, composite membranes. The reinforcement effect from GO-based graphene can mainly be attributed to its fine dispersion and strong interaction between the particles and the matrix. Moreover, the nanosheets may serve as connecting bridges to prevent the matrix from fracturing upon mechanical deformation, thus enhancing the MMM mechanical properties.

DMA was used to determine the glass transition temperature (Tg) via the maximum loss of applied energy; i.e. the loss factor or tan (δ) peak as a function of temperature as shown in Figure 10. The glass transition temperature of all the materials is listed in Table 3. Matrimid® 5218 polyimide has an aromatic group in the main chain substantially decreasing possible chain rotation and leading to a high Tg value (327 ºC as determined by DSC for the neat powder). However, in our case, the Tg of the Matrimid membrane was 315 ºC by DMA. Potentially, small molecules such as water and solvent are absorbed in the membrane, because the membranes were dried at 100 ºC only for 4 h, then the membranes were kept under ambient condition (40-65% humidity) before testing. When graphene particles are introduced between the main polymer chains, Tg is expected to increase due to lower macromolecular mobility. Typical tan δ results as a function of temperature are presented in Figure 10. The MMM Tg is very close to neat Matrimid as listed in Table 4. This may be due to the very low GO concentration used. Additionally, the one-atom-thick structures of the nanosheets are sufficiently flexible and have limited hindering ability on the polymer chains segmental motion, leading to negligible Tg variation.

**Table 4**
Young's modulus, elongation at break and Tg of the MMM.

| Materials | Young's modulus (GPa) | Elongation at break (%) | Tensile strength (MPa) | Tg (ºC) |
|---|---|---|---|---|
| **Neat Matrimid** | 2.26 | 49.0 | 80.5 | 315 |
| **M/GO0.1** | 2.40 | 9.8 | 82.7 | 314 |
| **M/TRGO0.3** | 2.39 | 7.9 | 79.1 | 314 |
| **M/TRGO0.5** | 2.47 | 5.8 | 83.0 | 313 |
| **M/AMP-RGO0.2** | 2.46 | 12.4 | 84.7 | 316 |
| **M/AMP-RGO0.4** | 2.50 | 7.5 | 83.0 | 315 |
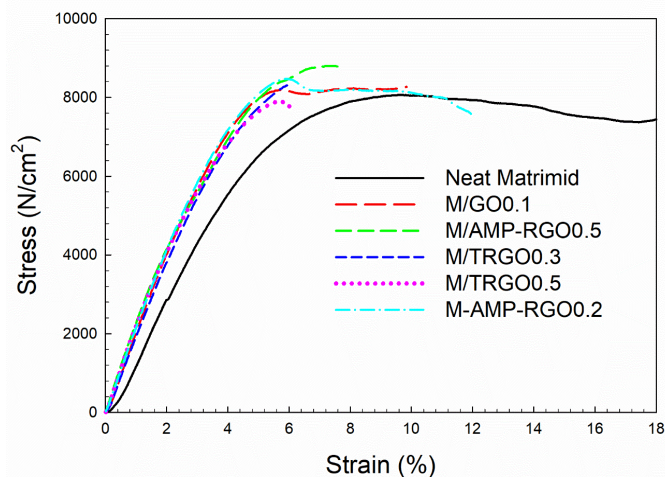


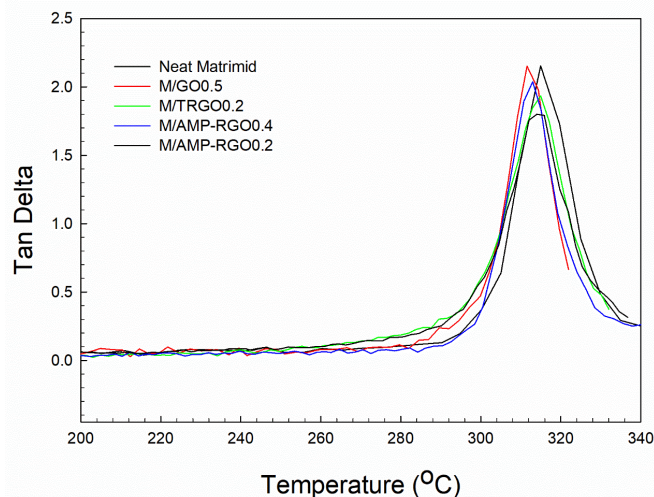**Fig. 10.** Loss factor (Tan delta) as a function of temperature for the MMM.

## 3.2. Gas transport properties

The MMM were expected to have improved separation performance compared to the neat polymer membranes as good particle dispersion was achieved. However, the MMM paradigm is faced with practical challenges due to the need to control factors limiting defects at the polymer-particle interfaces and MMM structures can be classified into four cases [38]: interfacial voids (sieves-in-a-cage), polymer rigidified chain layer near the molecular sieving particles, partial pore blockage and ideal case (no defect). Figure 11 presents the gas diffusion pathways in the MMM. Normally, gas molecules through polymer membranes follows the solution-diffusion model. Firstly, there is adsorption and dissolution of a number of gas molecules at the polymer interface (solubility coefficient). Then, these gas molecules diffuse into or through the polymer with different diffusion coefficients. Finally, the gas molecules desorb into the external phase. For graphene-polymer composite membranes, the graphene-layer influences the diffusion rate, while adsorption and desorption should not change. The carbon-carbon distance is only 1.42 Å so none of the gas molecules can transport through the graphene layer. Therefore, three routes are possible for the gas molecules to move in the composite membranes. The first one is molecular diffusion through the amorphous polymer phase as it is known that the crystalline regions are considered impermeable [39]. The second option, when the gases meet some resistance due to the graphene layer, the molecules need to change direction inside the polymer phase, but potentially meet again a graphene layer (tortuosity). The third route is for the gases to go through the interlayer space between the particle by Knudsen diffusion or molecular sieving effect depending on the distance between two layers and the molecule size. Obviously, in the second case, the gas transport rate is reduced by the presence of graphene and the gas diffusion rate decreases leading to lower permeability. On the other hand, the third case can increase or decrease the gas permeability. The gas molecules passing through the three GO was different. In M/GO, $H_2$, $CO_2$ and $O_2$ can pass the interlayer space between the graphene layers; In M/TRGO, only $H_2$ can pass the interlayer; while in M/AMP-RGO, $H_2$ and $CO_2$ can pass the interlayer. Therefore, the gas molecular transport for each membrane is discussed in the following section.

### 3.2.1. Matrimid/GO

The XRD analysis of GrO showed that six layers are present with an interlayer distance of 0.89 nm. When GrO is introduced into Matrimid after exfoliation by means of sonication (1 h), it is possible that the numbers of layers could be reduced as some polymer chains can enter these graphene layers. In that case the polymer chains would create a rigidified layer near these few-layer graphene, or produce partial pore blockage between two graphene layers. However, from the DMA analyses it was found that the MMM Tg was almost constant (see Table 4) so that significant rigidification did not occur in this case.
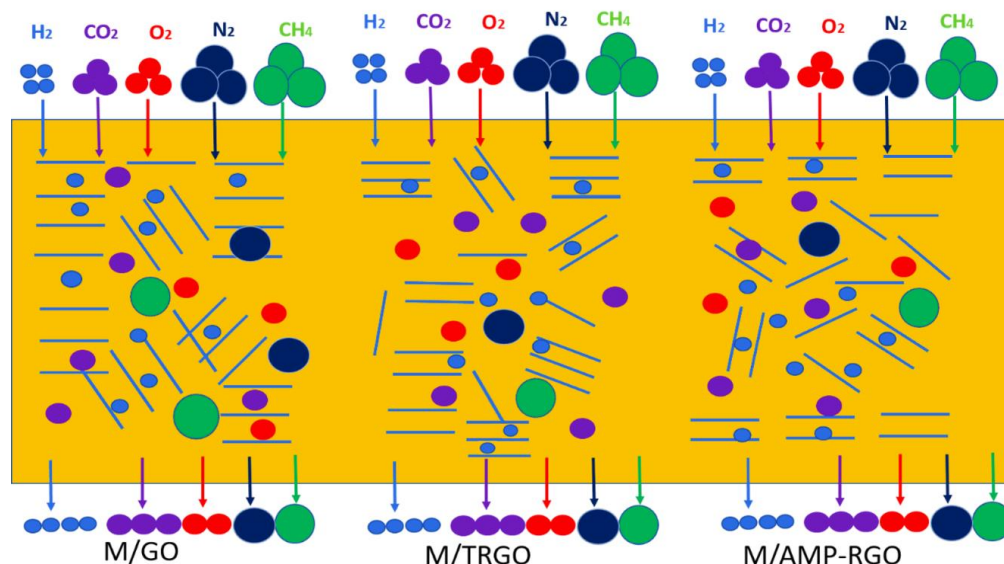


**Fig. 9.** Stress-strain curves of the MMM.

**Fig. 11.** Different gas diffusion pathways for the three different graphene-based composite membranes.

Figure 12 presents the gas permeation performance for Matrimid and graphene oxide composite membranes at 30 ℃ and 10 bar. For $H_2$ and $CO_2$ the permeability increased in M/GO compared to neat Matrimid. This result indicates that at 0.1wt.% GO loading where the diffusional change by tortuosity is not yet significant, some process involving an interaction between hydrogen and GO favors $H_2$ permeability. But with further GO content increase, the increased tortuosity is counteracting this effect. On the other hand, $O_2$, $N_2$ and $CH_4$ permeabilities slightly decreased compared with the neat Matrimid (exception for 1 wt.% M/GO). Based on the gas molecule sizes (2.98 Å for $H_2$, 3.30 Å for $CO_2$, 3.46 Å for $O_2$, 3.63 Å for $N_2$ and 3.80 Å for $CH_4$), and the distance between GO layers being approximately 8.9 Å for the GO concentration range studied (0.1 to 0.5 wt.%), the gas barrier effect is not controlled by the distance between GO layers. For 1 wt.% M/GO, GO agglomeration in the polymer matrix (see Figure 8) can produce more space between the layers letting all the gas molecules through leading to higher permeabilities. Therefore, in this case, the ideal selectivity of $H_2/N_2$, $H_2/CH_4$, $CO_2/N_2$ and $CO_2/CH_4$ slightly increased for 0.1-0.5 wt.% M/GO composite membranes, but decreased for 1 wt.% M/GO MMM (see Figure 12).

*3.2.2. Matrimid/T-RGO*

The XRD analysis of T-RGrO showed that three layers were present in a stack and the interlayer distance is 0.39 nm. Figure 13 presents the gas permeation performance for M/TRGO MMM at 30 ℃ and 10 bar. $H_2$ permeability was almost constant and similar to the neat Matrimid value. However, the most significant feature is the reproducible decrease in $CH_4$ permeability up to 0.2 wt.% T-RGO. This results in a significant increase in $H_2/CH_4$ ideal selectivity up to 226. Obviously this change is not associated with a tortuosity effect which would equally affect the permeability of the other gases tested. Note that $CH_4$ permeability in the neat Matrimid membrane was already very low (<0.5 Barrer) and that the presence of sonicated T-RGO seems to enhance this polymer lack of solubility for $CH_4$. $CO_2$ permeability was slightly decreased in MMM compared to neat Matrimid. It is assumed that $CO_2$ could not diffuse in the interlayer space of TRGO. Finally, $O_2$ and $N_2$ permeabilities were more decreased than in M/GO MMM. It is assumed that TRGO acts as a barrier for these larger molecules.

*3.2.3. Matrimid/AMP-RGO*

Figure 14 presents the gas permeation performance of M/AMP-RGO MMM at 30 ℃ and 10 bar. $H_2$ and $CO_2$ permeabilities were slightly increased for M/AMP-RGO 0.2 wt.% compared to the neat Matrimid. AMP-RGO was dispersed as mono-layer or two layers in the polymer. $H_2$ and $CO_2$ could possibly pass through the 4.1 Å interlayer, while $O_2$, $N_2$ and $CH_4$ permeabilities were even more decreased than in M/GO MMM. Therefore, the AMP-RGO acted as barrier for these three larger gas molecules.

The most important feature is again a large decrease in $CH_4$ permeability

at low (0.1 wt. %) AMP-RGO content in the membrane. This again resulted in a large increase in $H_2/CH_4$ selectivity which reached 231.
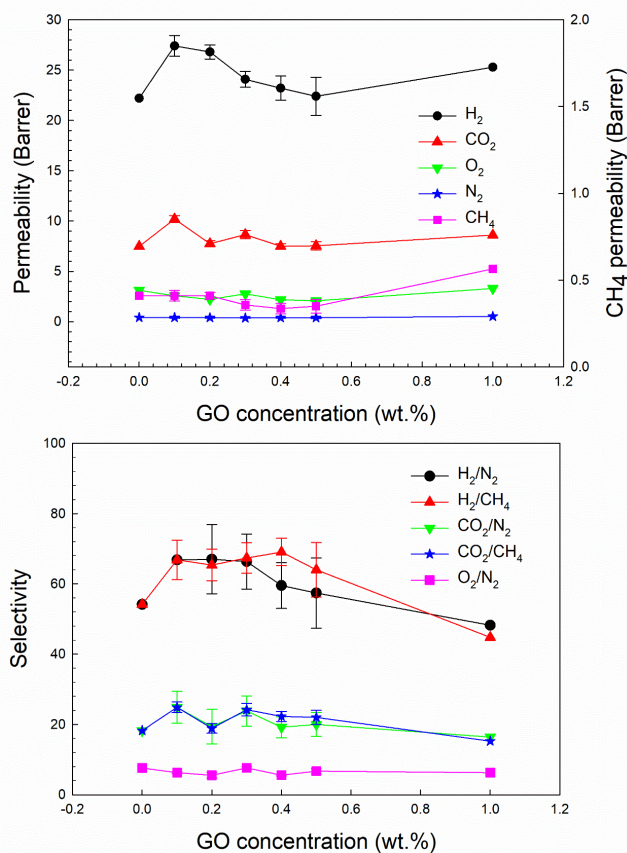




**Fig. 12.** MMM permeability (above) and ideal selectivity (below) as a function of GO concentration.
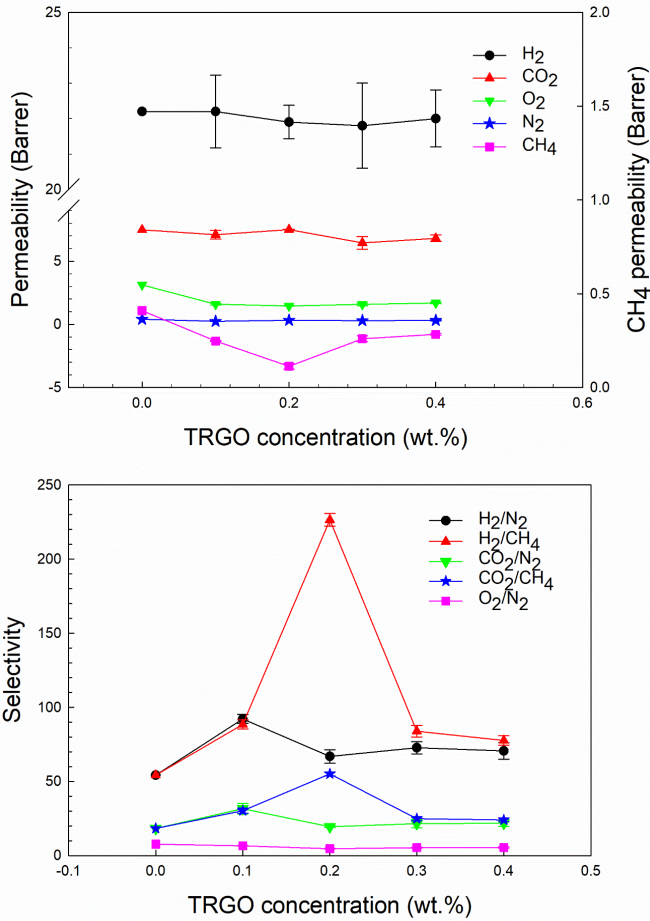
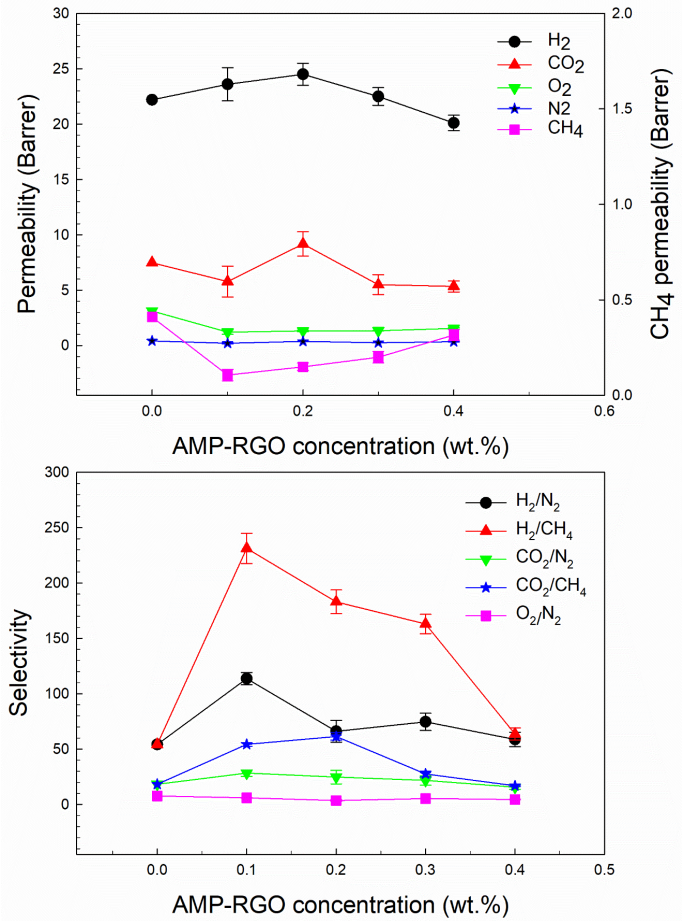**Fig. 13.** MMM permeability (above) and ideal selectivity (below) as a function of TRGO concentration.



**Fig. 14.** MMM permeability (above) and ideal selectivity (below) as a function of AMP-RGO concentration.

### 3.3. Comparison between the different GO/polymer MMM

#### 3.3.1. $CO_2/CH_4$ separation

The $CO_2/CH_4$ gas permeation performance of different polymer/GO MMM is presented in Figure 15 with respect to the Robeson upper bounds [41,42]. The black points are the results of this work and two points (M/AMP-RGO 0.1 and M/T-RGO 0.2) are close to the Robeson line 1991 ($P_{CO2}$ of 6.9, 7.5 Barrer and $CO_2/CH_4$ selectivity of 57 and 55). While one point for M/AMP-RGO 0.2 ($P_{CO2}$ of 10.7 and $CO_2/CH_4$ selectivity of 79.8) is above the Robeson 1991 line. The down triangles were obtained at 30 °C and 2 bar while the stars were obtained at 25 °C and 1.5 bar. Only one PDMS (up triangle) having very high $CO_2$ permeability also passed the first bound. It is known that gas selectivity decreases with increasing gas partial pressure. From our experience, some polyimides can lose more than 10% selectivity upon increasing the feed pressure from 2 to 10 bar [29]. Thus the data obtained under different feed pressures are difficult to compare.

#### 3.3.2. $H_2/CH_4$ separation

One work dealing with $H_2/CH_4$ separation by PDMS/GO MMM was found in the literature [20], and the data are compared to the results of this work in Figure 16. PDMS was good for $CO_2/CH_4$ and $CO_2/N_2$ separation because it is a rubbery polymer, but it is not good for the industrially important $H_2$ recovery. Two points of the Matrimid/GO (M/AMP-RGO 0.1 and M/T-RGO 0.2) series having high selectivity (231 and 226) and quite close to the Robeson bound (Figure 16). Therefore, these membranes are promising for industrial application. Keeping the high $H_2/CH_4$ selectivity (above 200), and using hollow fibers instead of flat MMM, the (permeance) could be improved by a reduction of the membrane thickness (skin layer) to the nano-scale.
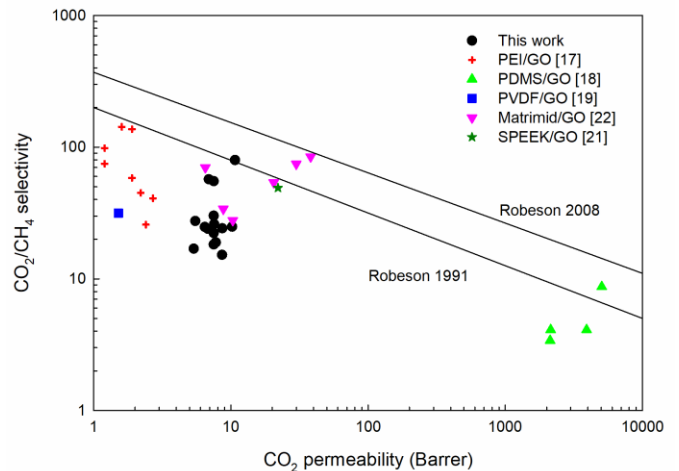


**Fig. 15.** Comparison of the $CO_2/CH_4$ separation performance of different polymer/GO MMM and Robeson upper bounds.

### 4. Conclusions

In this work, two new kinds of graphene based materials, thermally reduced graphite oxide (T-RGrO) and ascorbic acid multi-phase reduced graphene oxide (AMP-RGO), were synthesized and embedded in

Matrimid®5218 to produce mixed matrix membranes (MMM) for gas separation. As a first step, the carbon based materials were analyzed via XRD. The spectra showed that a [002] peak at a 2θ value of 23.0 and 22.1° was observed for T-RGrO and AMP-RGO, respectively. Therefore, the interlayer distance ($d_{002}$) were 0.39 and 0.41 nm, respectively.

The results showed that the gas molecules transported through the MMM in different ways depending on the gas molecular size and the MMM morphology (mainly the interlayer distance). The gas barrier effect was observed for larger gas molecules due to a narrow interlayer distance (T-RGrO and AMP-RGO). The result also showed that the AMP-RGO gas barrier effect was the highest, especially for $CH_4$, while $H_2$ and $CO_2$ were able to pass through the polymer phase and graphene interlayer. Therefore, the $CO_2/CH_4$ and $H_2/CH_4$ ideal selectivities reached values up to 79.8 and 231 respectively, which represents 344% and 328% improvements for M/AMP-RGO 0.2 and 0.1 compared to the neat matrix, respectively.

Therefore, these membranes are expected to be good starting point to optimize a methane separation process or biogas upgrading/natural gas purification system. The high selectivity for $H_2/CH_4$ and $H_2/N_2$ are also making these new membranes promising for several applications including hydrogen recovery from ammonia plants.
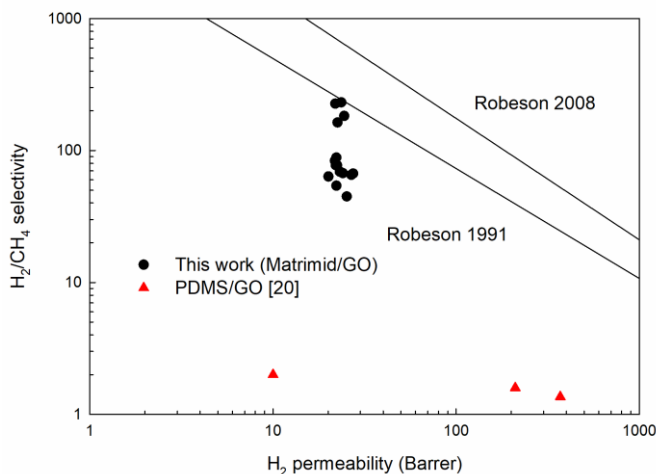


**Fig. 16.** Comparison of the $H_2/CH_4$ separation performance of different polymer/GO MMM and Robeson upper bounds.

### References

[1] K.S. Novoselov, A.K. Geim, S.V. Morozov, D. Jiang, Y. Zhang, S.V. Dubonos, I.V. Grigorieva, A.A. Firsov, Electric Field Effect in Atomically Thin Carbon Films, Science 306 (2004) 666-669.

[2] E. Bourgeat-Lami, J. Faucheu, A. Noel, Latex routes to graphene-based nanocomposites, Polym. Chem. 6 (2015) 5323-5357.

[3] C. Lee, X. Wei, J.W. Kysar, J. Hone, Measurement of the Elastic Properties and Intrinsic Strength of Monolayer Graphene, Science 321 (2008) 385-388.

[4] Y. Zhu, S. Murali, W. Cai, X. Li, J.W. Suk, J.R. Potts, R.S. Ruoff, Graphene and Graphene Oxide: Synthesis, Properties, and Applications, Adv. Mater. 2 (35) (2010) 3906-3924.

[5] H. Li, Z. Song, X. Zhang, Y. Huang, S. Li, Y. Mao, H.J. Ploehn, Y. Bao, M. Yu, Science 342 (2013) 95-98.

[6] H.W. Kim, H.W. Yoon, S.M. Yoon, B.M. Yoo, B.K. Ahn, Y.H. Cho, H.J. Shin, H. Yang, U. Paik, S. Kwon, J.Y. Choi, H.B. Park, Science 342 (2013) 91-95.

[7] B. Mi, Graphene Oxide Membranes for Ionic and Molecular Sieving, Science 343 (2014) 740-742.

[8] X.Y. Chen, O.G. Nik, D. Rodrigue, S. Kaliaguine, Polymer Mixed matrix membranes of aminosilanes grafted FAU/EMT zeolite and cross-linked polyimide for $CO_2/CH_4$ separation, Polymer 53 (2012) 3269-380.

[9] X.Y. Chen, S. Kaliaguine, D. Rodrigue, Correlation between Performances of Hollow Fibers and Flat Membranes for Gas Separation, Sep. & Purif. Rev. 47 (2018) 66-87.

[10] T.B. Nguyen, V.T. Hoang, X.Y. Chen, D. Rodrigue and S. Kaliaguine, Polymer functionalization to enhance interface quality of mixed matrix membranes for high $CO_2/CH_4$ gas separation, J. Mater. Chem. A. 3 (2015) 15202-15213.

[11] J. Shen, G. Liu, K. Huang, W. Jin, K.R. Lee, N. Xu, Membranes with Fast and Selective Gas-Transport Channels of Laminar Graphene Oxide for Efficient $CO_2$ Capture. Angew. Chem. Int. Ed. 54 (2015) 578-582.

[12] J. Shen, M. Zhang, G. Liu, K. Guan, W. Jin, Size Effects of Graphene Oxide on Mixed Matrix Membranes for $CO_2$ Separation, AIChE J. 62 (2016) 2843-2852.

[13] G. Dong, J. Hou, J. Wang, Y. Zhang, V. Chen, J. Liu, (2016) Enhanced $CO_2/N_2$ separation by porous reduced graphene oxide/Pebax Mixed matrix membranes, J. Membr. Sci. 520 (2016) 860-868.

[14] Y. Dai, X. Ruan, Z. Yan, K. Yang, M. Yu, H. Li, W. Zhao, G. He, Imidazole functionalized graphene oxide/PEBAX mixed matrix membranes for efficient $CO_2$ capture, Sep. Purif. Technol. 166 (2016) 171-180.

[15] L.G. Wu, C.H. Yang, T. Wang, X.Y. Zhang, Enhanced the performance of graphene oxide/polyimide hybrid membrane for $CO_2$ separation by surface modification of graphene oxide using polyethylene glycol, Appl. Surf. Sci. 440 (2018) 1063-1072.

[16] B.S. Ge, T. Wang, H.X. Sun, W. Gao, H.R. Zhao, Preparation of mixed matrix membranes based on polyimide and aminated graphene oxide for $CO_2$ separation, Polym. Adv. Technol. 29 (2018) 1334-1343.

[17] H. Koolivand, A. Sharif, M.R. Kashani, M. Karimi, M.K. Salooki, M.A. Semsarzadeh, Functionalized graphene oxide/polyimide nanocomposites as highly $CO_2$-selective membranes, J. Polym. Res. 21 (2014) 599-610.

[18] H. Koolivand, A. Sharif, E. Chehrazi, M.R. Kashani, S.M.R. Paran, Mixed-Matrix Membranes Comprising Graphene-Oxide Nanosheets for $CO_2/CH_4$ Separation: A Comparison Between Glassy and Rubbery Polymer Matrices, Polym. Sci. Ser. A, 58 (2016) 801-809.

[19] E.A. Feijani, A. Tavassoli, H. Mahdavi, H. Molavi, Effective gas separation through graphene oxide containing mixed matrix membranes, J. Appl. Polym. Sci. 135 (2018) 46271-46280.

[20] H. Ha, J. Park, S. Ando, C.B. Kim, K. Nagai, B.D. Freeman, C.J. Ellison, Gas permeation and selectivity of poly(dimethylsiloxane)/graphene oxide composite elastomer membranes, J. Membr. Sci. 518 (2016) 131-140.

[21] Q. Xin, Z. Li, C. Li, S. Wang, Z. Jiang, H. Wu, Y. Zhang, J. Yange, X. Cao, Enhancing the $CO_2$ separation performance of composite membranes by the incorporation of amino acid-functionalized graphene oxide, J. Mater. Chem. A. 3 (2015) 6629-6641.

[22] X. Li, L. Ma, H. Zhang, S. Wang, Z. Jiang, R. Guo, H. Wu, X. Cao, J. Yang, B. Wang, Synergistic effect of combining carbon nanotubes and graphene oxide in mixed matrix membranes for efficient $CO_2$ separation, J. Membr. Sci. 479 (2015) 1-10.

[23] A. Melicchioa, P.F. Evangelos, Preparation and characterization of graphene oxide as a candidate filler material for the preparation of mixed matrix polyimide membranes, Surf. Coat. Technol. 349 (2018) 1058-1068.

[24] W.S. Hummers Jr, R.E. Offeman, Preparation of graphitic oxide, J. Am. Chem. Soc. 80 (1958) 1339-1339.

[25] J. Zhang, H. Yang, G. Shen, P. Cheng, S. Guo, Reduction of graphene oxide via ascorbic acid, Chem. Commun. 46 (2010) 1112-1114.

[26] M.P. Lavin-Lopez, A. Paton-Carrero, L. Sanchez-Silva, J.L. Valverde, A. Romero, Influence of the reduction strategy in the synthesis of reduced graphene Oxide, Adv. Powder Technol. 28 (2017) 3195-3203.

[27] L. Stobinski, B. Lesiak, A. Malolepszy, M. Mazurkiewicz, B. Mierzwa, J. Zemek, P. Jiricek, I. Bieloshapka, Graphene oxide and reduced graphene oxide studied by the XRD, TEM and electron spectroscopy methods, J. Electron Spectrosc. Relat. Phenom. 195 (2014) 145-154.

[28] B.E. Warren, X-ray diffraction in random layer lattices, Phys. Rev. 59 (1941) 693-698.

[29] X.Y. Chen, D. Rodrigue, S. Kaliaguine, Diamino-organosilicone APTMDS: A new cross-linking agent for polyimides membranes, Sep. Purif. Technol. 86 (2012) 221-233.

[30] X.Y. Chen, S. Kaliaguine, Mixed Gas and Pure Gas Transport Properties of Copolyimide Membranes, J. Appl. Polym. Sci. 128 (2013) 380-389.

[31] C.K. Chua, M. Pumera, M. The reduction of graphene oxide with hydrazine: elucidating its reductive capability based on a reaction-model approach, Chem. Commun. 52 (2016) 72-75.

[32] L.Y. Jiang, T.S. Chung, Homogeneous Polyimide/Cyclodextrin Composite Membranes for Pervaporation Dehydration of Isopropanol, J. Membr. Sci. 346 (2010) 45-48.

[33] M.J. Fernández-Merino, L. Guardia, J.I. Paredes, S. Villar-Rodil, P. Solís-Fernández, A. Martínez-Alonso, J.M.D. Tascón, Vitamin C is an ideal substitute for hydrazine in the reduction of graphene oxide suspensions, J. Phys. Chem. C 114 (2010) 6426-6432.

[34] V. Loryuenyong, K. Totepvimarn, P. Eimburanapravat, W. Boonchompoo, A. Buasri, Preparation and characterization of reduced graphene oxide sheets via water-based exfoliation and reduction methods, Adv. Mater. Sci. Eng. 2013 (2013) 1-5.

[35] M.J. McAllister, J.L. Li, D.H. Adamson, H.C. Schniepp, A.A. Abdala, J. Liu, M. Herrera-Alonso, D.L. Milius, R. Car, R.K. Prud'homme, I.A. Aksay, Single sheet functionalized graphene by oxidation and thermal expansion of graphite, Chem. Mater. 19 (2007) 4396-4404.

[36] Y. Liu, R. Wang, T.S. Chung, Chemical cross-linking modification of polyimide membranes for gas separation, J. Membr. Sci. 189 (2001) 231-239.

[37] J.N. Barsema, S.D. Klijnstra, J.H. Balster, N.F.A. van der Vegt, G.H. Koops, M. Wessling, Intermediate polymer to carbon gas separation membranes based on Matrimid PI, J. Membr. Sci. 238 (2004) 93-102.

[38] D.Q. Vu, W.J. Koros, Mixed matrix membranes using carbon molecular sieves I. Preparation and experimental results, J. Membr. Sci. 211 (2003) 311-334.

[39] M. Rezakazemi, A.E. Amooghin, M.M. Montazer-Rahmati, A.F. Ismail, T. Matsuura, State-of-the-art membrane-based $CO_2$ separation using mixed matrix membranes (MMMs): An overview on current status and future directions, Prog. Polym. Sci. 39 (2014) 817-861.

[40] S. Zekriardehani, S.A. Jabarin, D.R. Gidley, M.R. Coleman, Effect of Chain Dynamics, Crystallinity, and Free Volume on the Barrier Properties of Poly(ethylene terephthalate) Biaxially Oriented Films, Macromolecules 50 (2017) 2845-2855.

[41] L.M. Robeson, Correlation of separation factor versus permeability for polymeric membranes, J. Membr. Sci. 62 (1991) 165-185.

[42] L.M. Robeson, The upper bound revisited, J. Membr. Sci. 320 (2008) 390-400.